UC Davis
UC Davis Previously Published Works

Title

The E3 Ubiquitin Ligase MIB-1 Is Necessary To Form the Nuclear Halo in Caenorhabditis elegans Sperm

Permalink

https://escholarship.org/uc/item/3bc5n962

Journal

G3: Genes, Genomes, Genetics, 8(7)

ISSN

2160-1836

Authors

Herrera, Leslie A
Starr, Daniel A

Publication Date

2018-07-01

DOI

10.1534/g3.118.200426

Peer reviewed

The E3 Ubiquitin Ligase MIB-1 Is Necessary To Form the Nuclear Halo in *Caenorhabditis elegans* Sperm

Leslie A. Herrera and Daniel A. Starr[1]
Department of Molecular and Cellular Biology, University of California, Davis, CA 95616
ORCID ID: 0000-0001-7339-6606 (D.A.S.)

ABSTRACT Unlike the classical nuclear envelope with two membranes found in other eukaryotic cells, most nematode sperm nuclei are not encapsulated by membranes. Instead, they are surrounded by a nuclear halo of unknown composition. How the halo is formed and regulated is unknown. We used forward genetics to identify molecular lesions behind three classical *fer* (fertilization defective) mutations that disrupt the ultrastructure of the *Caenorhabditis elegans* sperm nuclear halo. We found *fer-2* and *fer-4* alleles to be nonsense mutations in *mib-1*. *fer-3* was caused by a nonsense mutation in *eri-3*. GFP::MIB-1 was expressed in the germline during early spermatogenesis, but not in mature sperm. *mib-1* encodes a conserved E3 ubiquitin ligase homologous to vertebrate Mib1 and Mib2, which function in Notch signaling. Here, we show that *mib-1* is important for male sterility and is involved in the regulation or formation of the nuclear halo during nematode spermatogenesis.

One hallmark of eukaryotic cells is the nuclear envelope, a specialized extension of the endoplasmic reticulum consisting of two lipid bilayers and a perinuclear space (Hetzer 2010). The essential role of the nuclear envelope is to compartmentalize the nucleus from the cytoplasm. Therefore, the nuclear envelope evolved in the last eukaryotic common ancestor and was critical to the evolution of the wide variety of eukaryotic organisms alive today (Baum and Baum 2014). However, there are exceptions to this paradigm. All nematode classes except Enoplida have sperm devoid of a nuclear envelope at maturity (Justine 2002; Yushin and Malakhov 2014). Instead of two lipid bilayers, nematode sperm nuclei are surrounded by a halo of electron-dense material that also encapsulates the sperm centrioles (Wolf *et al.* 1978). The halo is thought to contain RNA (Ward *et al.* 1981).

Nearly forty years after its initial discovery, little is known about the molecular makeup and developmental regulation of the perinuclear halo. Two components have been shown to localize to the nuclear halo, the centrosome component SPD-2 and the novel protein SPE-11, which is one of the few paternally provided proteins in the embryo (Browning and Strome 1996; Sadler and Shakes 2000; McNally *et al.* 2012), but any role of these two proteins in the organization of the nuclear halo is unknown. One intriguing hypothesis is that the sperm nuclear halo serves as a sink for paternally provided mRNA, siRNA, and piRNA molecules that are delivered to the zygote through sperm (Stoeckius *et al.* 2014). Here, we employed a forward genetic approach in *C. elegans* to identify additional players in the formation of the perinuclear halo of nematode sperm.

C. elegans has long been appreciated as an excellent model to study gametogenesis (Hirsh *et al.* 1976). A large number of mutations have been isolated in *C. elegans* genes required for spermatogenesis, called *fer* or *spe* for <u>fer</u>tilization or <u>spe</u>rmatogenesis defective, respectively (Argon and Ward 1980; L'Hernault *et al.* 1988). These mutations are specific to spermatogenesis and result in hermaphrodites that lay unfertilized oocytes. The temperature sensitive period for *fer* mutants corresponds to the timing of spermatogenesis in hermaphrodites and the fertilization defect can be rescued by mating mutant hermaphrodites to wild-type males (Argon and Ward 1980).

We were particularly interested in three genes, *fer-2*, *fer-3*, and *fer-4*, because of their striking ultrastructural mutant phenotype (Ward *et al.* 1981). When sperm from *fer-2*, *fer-3*, or *fer-4* mutant males grown at 25° are examined by electron microscopy, the RNA halo that normally surrounds centrioles and condensed chromatin in mature spermatids is absent (Ward *et al.* 1981). In place of the halo, large tubules of straight hollow cylinders accumulate around the condensed chromatin of spermatids and sperm (Ward *et al.* 1981). The nature of the perinuclear tubules is unknown; with diameters of about 50 nm (Ward *et al.* 1981), they are unlike other described tubular cellular components. The

[1]Correspondence to: 1 Shields Ave, Department of Molecular and Cellular Biology, University of California, Davis, Davis, CA 95616, E-mail: dastarr@ucdavis.edu

working model, as proposed by Ward *et al.* (1981), is that in *fer-2*, *fer-3*, or *fer-4* mutant sperm, tubules form from aberrant polymerized components of the ribonucleoprotein complexes that normally make the perinuclear halo. We hypothesized that determining the molecular identity of *fer-2*, *fer-3*, and *fer-4* gene products would elucidate molecular mechanisms of the formation of the normal perinuclear halo and/or the abnormal tubules that form in the mutant sperm. Here we report that *fer-2* and/or *fer-4* is a mutation in the predicted E3 ubiquitin ligase *mib-1* and that *fer-3* is a mutation in *eri-3*, a member of a Dicer-associated complex.

MATERIALS AND METHODS

Strains

C. elegans strains were grown on nematode growth medium plates spotted with OP50 bacteria and maintained at 15° unless otherwise noted (Stiernagle 2006). N2 was used as the wild-type control strain (Brenner 1974). Strains were provided by the Caenorhabditis Genetics Center, which is funded by the National Institutes of Health Office of Research Infrastructure Programs (P40 OD010440). Strains BA2 *fer-2 (hc2)*, BA3 *fer-3(hc3)*, BA4 *fer-4(hc4)*, BA547 *fer-2(hc2)*; *him-5(e1490)*, and BA562 *fer-4(hc4)*; *him-5(e1490)* were previously described (Argon and Ward 1980). WM172 *eri-3(tm1361)* II was originally made by Shohei Mitani (National Bioresource Project at the Tokyo Women's Medical University).

Whole genome sequencing

For genomic DNA preps, nearly starved animals from five plates (5 cm each) were washed in M9 (Stiernagle 2006), pelleted, resuspended in 200 μL buffer ATL (QIAGEN), and subjected to three freeze-thaw cycles. Genomic DNA was purified following the "animal tissue" protocol of the QIAGEN DNeasy Blood & Tissue Kit with an added RNAse A (10 mg/ml) incubation at room temperature for 15 min after the Proteinase K incubation. Genomic DNA was sent to the Functional Genomics Laboratory at QB3-Berkeley, fragmented into 300-600 bp pieces, and cloned into multiplexed libraries. The libraries were sequenced using paired end reads of 150 base pairs on an Illumina HiSeq 2500. Sequences were aligned, filtered and tabulated following the CloudMap pipeline (Minevich *et al.* 2012) on the public Galaxy server (Afgan *et al.* 2016).

CRISPR/Cas9 mutagenesis and genome editing

CRISPR/Cas9 was used to generate a null mutation in *mib-1* and to fuse *gfp* to the 5′ or 3′ end of the *mib-1* open reading frame (Paix *et al.* 2015; 2016). Custom guide crRNA and universal tracrRNA were synthesized by Integrated DNA Technologies or Dharmacon. For the *mib-1(yc44)* mutation, the crRNA guide sequence was CGUAAUACCACCUC-GAAAAC. For the *mib-1::gfp(yc46)* fusion, the sequence of the crRNA was AUUGAUAUUCACGAGUAGAU. For *gfp::mib-1(yc51)* we used ACAAAAAUGAACGGAGUAGC as the crRNA. Purified Cas9-NLS protein was obtained from QB3-Berkeley. To make the repair templates for the homology-directed insertion, *gfp* sequences were amplified from pDD282 (a gift from Bob Goldstein; Addgene plasmid # 66823) (Dickinson *et al.* 2015) using Phusion DNA Polymerase (Thermo Fisher Scientific) and primers with overhangs consisting of 58-60 base pairs of *C. elegans* homology flanking the predicted CRIPSR/Cas9 cut-site (Paix *et al.*, 2015). The QIAquick PCR Purification Kit (Qiagen) was used to clean the PCR product. In brief, we injected young adult hermaphrodite gonads with 9 μM or 17.5 μM crRNA:tracrRNA:Cas9 complexes along with 0.67 μM of the repair template for the *gfp* insertions (Paix *et al.* 2015; 2016). To follow CRISPR efficiency we used the *dpy-10* co-CRISPR approach (Arribere *et al.* 2014). Both a *dpy-10* crRNA sequence (1:12 ratio for *dpy-10* crRNA:*mib-1* crRNA) and 0.5 μM ssDNA oligo as a *dpy-10* repair template were added to the injection mix (Arribere *et al.* 2014). The *dpy-10* mutation was removed from the strains by crossing to N2 or *him-8(e1489)* males. The following three strains were generated: UD549 *mib-1(yc44)*; UD563 *mib-1::gfp(yc46)*; *him-8(e1489)*, and UD577 *gfp::mib-1(yc51)*, *him-8(e1489)*.

Fertilization and brood size phenotypes

To quantify the temperature-sensitive fertilization defects, assayed strains were initially cultured at 15° on NGM plates seeded with OP50. Twenty L2 hermaphrodites from each strain were singled onto their own plates. For the *hc2/yc44* complementation test, we singled 40 F1 L2s expecting half would be males. Half of singled L2s were then raised at 25° and the other half at 15°. After 48 hr, hermaphrodites raised at 25° were transferred to a fresh plate. The oocytes remaining on the original plate were scored as "fertilized" or "not fertilized" based on the globular and opaque appearance of unfertilized oocytes and the development of fertilized oocytes into L1 progeny within 24 hr. Oocytes laid within a 2-day window were added together. Plates with less than a total of 25 oocytes were excluded from the data. Also excluded were counts from F1s that were not cross progeny, which was verified by Sanger sequencing. For L2s raised at 15°, counts started 72 hr after individuals were singled to account for the delay in development.

Microscopy

We performed immunofluorescence staining on dissected male germlines from L4 males grown at 20°. Dissection, fixation and immunofluorescence were performed as described (Jaramillo-Lambert *et al.* 2007) with the following alterations. Samples were fixed for 5 min at room temperature in 2% paraformaldehyde in egg buffer [118 mM NaCl, 48 mM KCl2, 2 mM CaCl2, 2 mM MgCl2, 5 mM HEPES at pH 7.4]. We used a 0.7% BSA/1x PBS + 0.1% Tween20 solution for blocking. Rabbit anti-GFP antibody (NovusBiologicals NB600-308) was used at a 1:500 dilution and donkey anti-rabbit antibody Alexa Fluor 488 (Invitrogen A21206) was used at 1:500 for the secondary. DNA was stained with DAPI (final concentration of 0.2 ng/uL). Images were collected with a 63× Plan Apo 1.40 NA objective on an DM6000 epifluorescence compound microscope (Leica) with AF6000 software (Leica). Images were uniformly enhanced using the levels command in Adobe Photoshop.

Data Availability

Strains and plasmids are available upon request. The authors affirm that all data necessary for confirming the conclusions of the article are present within the article and figures.

RESULTS AND DISCUSSION

fer-2 is a mutation in mib-1

We set out to identify the molecular lesions of *fer-2*, *fer-3*, and *fer-4* using a whole-genome sequencing approach. Libraries were prepared from *fer-2(hc2)* or *fer-3(hc3)* genomic DNA for Illumina paired-end sequencing. The sequences were aligned and analyzed using the CloudMap pipeline (Minevich *et al.* 2012) which identified over 5,000 single nucleotide polymorphisms (SNP) in the sequenced *fer-2(hc2)* strain when compared to the reference N2, wild-type genome. Only a single SNP in the *fer-2(hc2)* sequence data set was predicted to cause a nonsense mutation in an open reading frame. This SNP was a C to T transition at position 11,297,830 of chromosome III. It is predicted to change the tryptophan of codon number 460 in the *mib-1* gene to a stop codon. Thus, we hypothesized that *fer-2(hc2)* is an allele of *mib-1*.
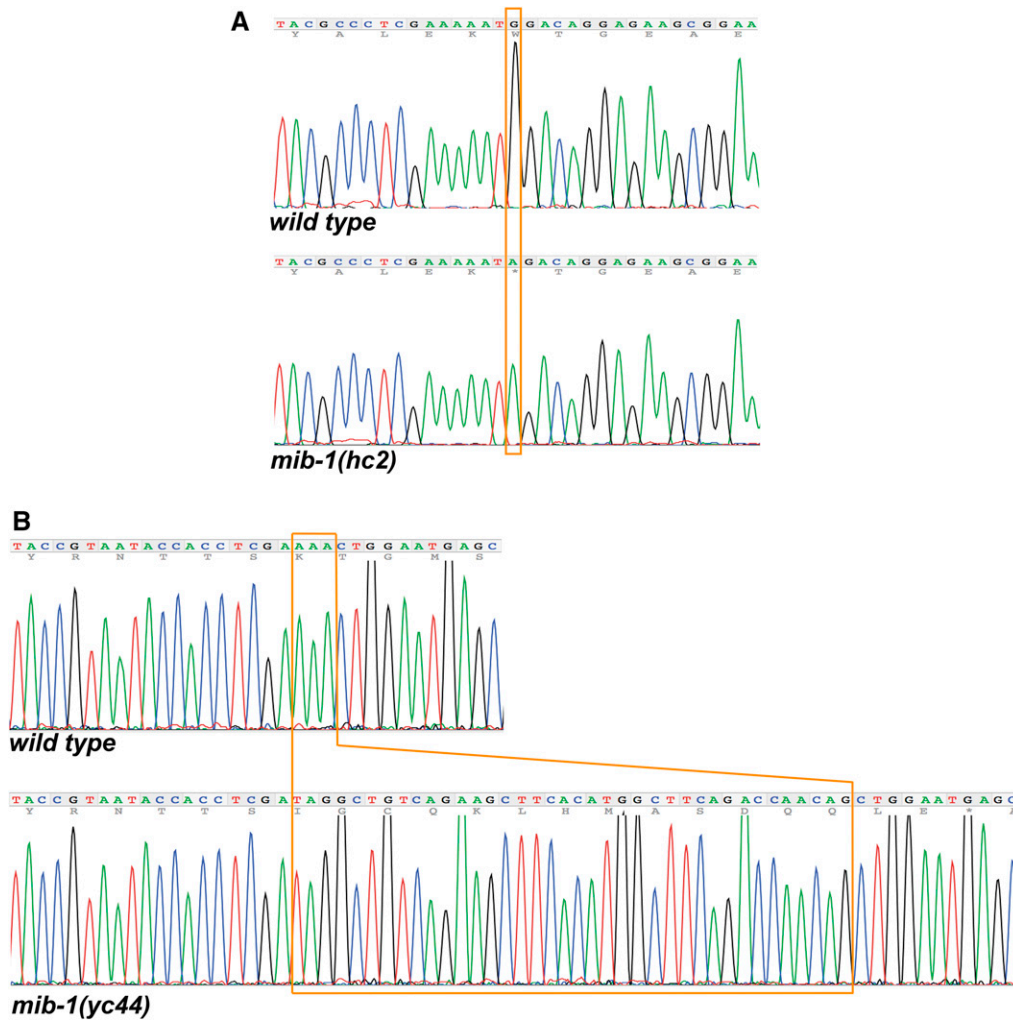
Figure 1 Mutations in *mib-1*. Sanger sequence outputs for wild type and *mib-1* mutant strains. (A) *hc2* is a C to T transition at position 11,297,830 of chromosome III. The opposite coding strand sequence is shown that leads to a Tryptophan to stop codon nonsense mutation. (B) *yc44* is a 38 bp insertion (boxed) in the sixth exon of *mib-1* that is quickly followed by a stop codon.

We have high confidence in the *mib-1* mutation for the following three reasons. 1. The mutation was covered 105 times in the whole-genome dataset and confirmed by Sanger sequencing (Figure 1A). 2. Although *fer-2* was originally mapped to chromosome IV (Argon and Ward 1980), three-point mapping later placed *fer-2* between *tra-1* and *dpy-18*, close to position 7.2 cM on chromosome III (Hodgkin 1993). This position is within a cM of *mib-1*. 3. Based on the *fer-2(hc2)* phenotype, we predicted that *fer-2* transcripts would be enriched in the male germline. We therefore examined a list of 864 spermatogenesis-enriched genes previously identified in a microarray study (Reinke *et al.* 2004). *mib-1* is the only one of the 864 transcripts that maps between *tra-1* and *dpy-18* on chromosome III. Thus, *fer-2* maps near *mib-1* and *mib-1* is the only gene in the region enriched in spermatogenesis expression lists.

To further test whether *fer-2* is *mib-1*, one would traditionally attempt to rescue *fer-2(hc2)* with wild-type genomic DNA of the *mib-1* locus or to phenocopy the *fer-2(hc2)* phenotype with *mib-1(RNAi)*. However, extrachromosomal arrays are suppressed in germ lines and RNAi is very inefficient in *C. elegans* sperm. In addition, no known alleles of *mib-1* had been previously identified or characterized. We therefore generated a new insertion/deletion allele of *mib-1* through imprecise non-homologous end joining repair after inducing a double strand break using CRISPR/Cas9. We isolated a mutant allele, *mib-1(yc44)* with a 38 base pair insertion of the *dpy-10* repair template that was used in our co-CRISPR

approach (Arribere *et al.* 2014). The *yc44* insertion into the sixth exon of *mib-1* is predicted to cause a frame shift and is therefore likely a null allele (Figure 1B). *mib-1(yc44)* animals laid about 18% unfertilized oocytes when raised at 15°, but laid an average of 97% unfertilized oocytes at 25° (Figure 2). Thus, *mib-1(yc44)* phenocopied *fer-2(hc2)* as a temperature-sensitive spermatogenesis defective mutant.

As final confirmation that *fer-2(hc2)* is an allele of *mib-1*, we crossed males homozygous for the C to T SNP on chromosome III to *mib-1(yc44)* hermaphrodites, and raised the F1 progeny at 25°. The *fer-2(hc2)/mib-1(yc44)* heterozygotes laid 97.8% unfertilized oocytes at the restrictive temperature (Figure 2). Thus, *fer-2(hc2)* failed to complement *mib-1(yc44)* and we concluded that *hc2* is an allele of *mib-1*.

Our results suggest that one *fer-2(hc2)* strain has been mislabeled since its original isolation (Argon and Ward 1980). We ordered all available strains carrying *hc2* or *hc4* from the Caenorhabditis Genetics Center and sequenced *mib-1* for the C to T mutation that causes the premature stop codon (Figure 1A) that we found in *hc2*. We identified the C to T mutation in BA2 *fer-2(hc2)*, BA4 *fer-4(hc4)*, and BA562 *fer-4(hc4)*; *him-5(e1490)*. However, the mutation was absent in BA547 *fer-2(hc2)*; *him-5(e1490)*. Thus, an unidentified different lesion, perhaps outside of *mib-1*, likely causes the temperature-sensitive male sterile phenotype in the BA547 strain and it is not possible to determine whether we identified the original *fer-2(hc2)* or *fer-4(hc4)* lesion. We henceforth refer to both *fer-2* and *fer-4* as *mib-1*.
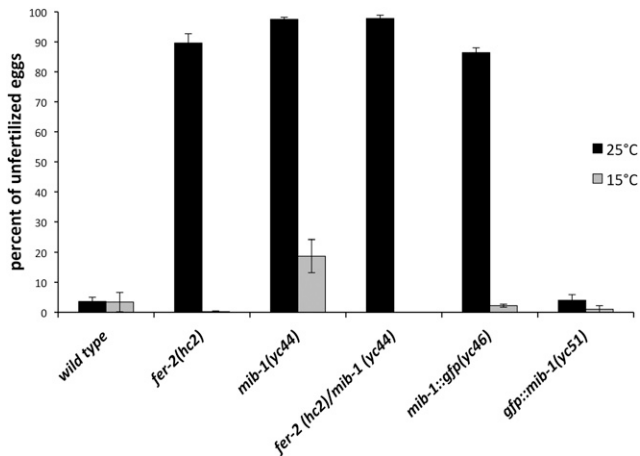
Figure 2 *mib-1* is required for male fertility. The mean percent of unfertilized oocytes from the total number of oocytes plus embryos laid by hermaphrodites is shown. For each bar, progeny from at least 10 hermaphrodites were scored at 15° and 25°C. Error bars are the standard error of the mean.

Localization of MIB-1 during spermatogenesis

After determining the *fer-2* phenotype was due to a mutation in *mib-1*, CRISPR/Cas9 gene editing was used to tag the C-terminus of endogenous MIB-1 with GFP. Animals homozygous for *mib-1::gfp(yc46)* as the only source of MIB-1 lay an average of 86% unfertilized oocytes at 25° (Figure 2), suggesting that MIB-1::GFP is nonfunctional. We proceeded to use CRISPR/Cas9 to tag MIB-1 with GFP at the N-terminus. *gfp::mib-1(yc51)* hermaphrodites laid wild-type percentages of fertilized embryos at both the permissive and restrictive temperatures (Figure 2), suggesting GFP::MIB-1 is functional. We next visualized GFP::MIB-1 by immunofluorescence with anti-GFP antibodies because of a weak GFP signal in live animals. GFP::MIB-1 was highly expressed in the proximal arm of the male gonad, but not in mature sperm (Figure 3). The timing of GFP::MIB-1 expression was consistent with a role in

spermatogenesis. We observed cytoplasmic GFP::MIB-1 expression starting at mid-pachytene of male gonads. The signal persisted throughout late pachytene, diplotene, and diakinesis. The last visible signal detected was in the cytoplasmic residual body. We did not detect GFP::MIB-1 in mature spermatids. GFP::MIB-1 is similarly expressed in the L4 hermaphrodite gonad during spermatogenesis. The nuclear halo is formed shortly after spermatids bud off the residual body (Wolf *et al.* 1978; Ward *et al.* 1981). Thus, the timing of expression and the depositing of GFP::MIB-1 into the residual body is consistent with a model where MIB-1 needs to be turned off to stabilize its targets and allow its targets to function in the normal formation of the nuclear halo. In *mib-1* mutants, the targets would be prematurely active, leading to the gross ultrastructural deformities previously described for *fer-2* and *fer-4* (Ward *et al.* 1981).

Possible mechanisms for MIB-1 and the sperm nuclear halo

C. elegans mib-1 encodes an E3 ubiquitin protein ligase conserved to vertebrate Mib1 and Mib2 (Berndt *et al.* 2011). Mutations in the human *MIB1* gene cause left ventricular noncompaction cardiomyopathy (Luxán *et al.* 2013). Mib1 ubiquitinates the Notch ligands Delta and Jagged and targets them for endocytosis, turning off Notch signaling in zebrafish and mammals (Itoh *et al.* 2003; Kang *et al.* 2013). However, there are no major Notch-related phenotypes reported in $MIB2^{-/-}$ knockout mice, suggesting that Mib2 acts synthetically to regulate Notch signaling and/or targets at least one alternate substrate (Koo *et al.* 2005; Guo *et al.* 2016). Our results show that *C. elegans mib-1* mutants have a fertilization defective phenotype that is distinct from any previously described Notch pathway mutant in *C. elegans* (Greenwald 2005). Thus, it appears that *mib-1* has an additional role in nematodes to function in perinuclear halo formation during spermatogenesis. A recent report showed that lesions in *mib-1* are also the cause of the *spe-16(hc54)* spermatogenesis-defective phenotype (Ratliff *et al.* 2018). A phenotypic analysis of *spe-16* showed that it had the same temperature-dependent, male-sterile phenotype as previously reported for *fer-2* and *-4* (Ratliff *et al.* 2018), but whether *spe-16* disrupts the
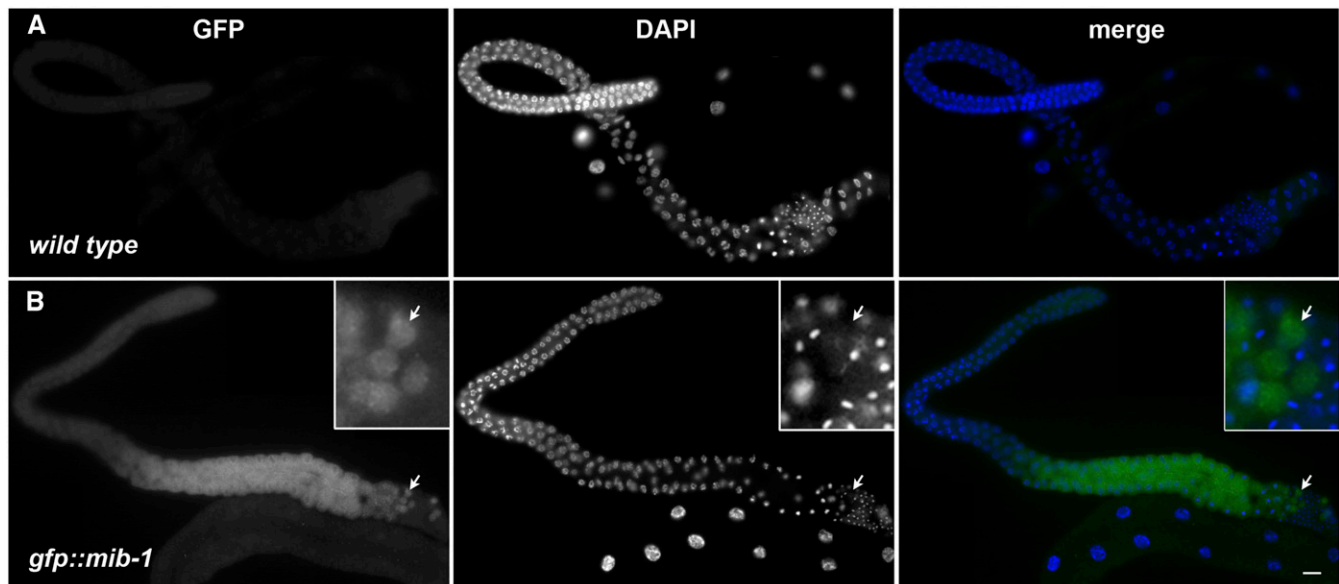
Figure 3 GFP::MIB-1 is expressed in the male germline. (A) wild type and (B) *gfp::mib-1*. Anti-GFP immunofluorescence showing GFP::MIB-1 expression in the proximal arm of male germline. GFP is green and DAPI-stained nuclei are blue in the merge. Scale bar is 10 μm. In the inset, a group of four residual bodies marked with an arrow is enlarged.

formation of the sperm nuclear halo was not tested. Similar to our findings, Ratliff *et al.* (2018) showed that GFP::MIB-1 localized diffusely in the male germline, but not in sperm. In addition, they found that *mib-1* has a function in the Delta/Notch pathway, as loss-of-function alleles of *mib-1* partially suppressed gain-of-function *lin-12* vulva developmental defects (Ratliff *et al.* 2018). Finally, Ratliff *et al.* (2018) showed that MIB-1 can ubiquitinate itself *in vitro*. However, the exact *in vivo* target(s) of MIB-1 during spermatogenesis and nuclear halo formation remains to be determined.

We also cloned *fer-3(hc3)* by whole-genome sequencing. We had very little mapping data to guide us for *fer-3*. However, scanning the CloudMap output of SNPs between *fer-3(hc3)* and wild type led to the identification of a nonsense mutation in *eri-3*. We found a T to C transition at position 1,123,966 of chromosome II, which changes codon 69 of the *eri-3* gene from a serine to a proline. *eri-3* was previously reported to have a temperature sensitive spermatogenesis mutant phenotype (Pavelec *et al.* 2009). We crossed *fer-3(hc3)* into *eri-3 (tm1361)* and the alleles failed to complement; F1 heterozygote hermaphrodites laid unfertilized embryos at 25°. An additional group also reported that *fer-3(hc3)* is an allele of *eri-3* using the same complementation test (Conine *et al.* 2013). ERI-3 is a component of the 26G-RNA ALG-3/4 pathway and mutations in *alg-3/4* lead to a similar nuclear halo defect in spermatozoa, suggesting that they are in the same pathway (Conine *et al.* 2013). Perhaps, MIB-1 and ERI-3 function to load specific paternal RNAs into the nuclear halo of sperm that are then contributed to the zygote (Stoeckius *et al.* 2014). The expression of MIB-1 during spermatogenesis and a common downstream phenotype suggests a potential role in post-transcriptional regulation of proteins required for normal sperm morphology. It could therefore be informative in the future to identify the targets of MIB-1 and any possible relationship between MIB-1 and the 26G-RNA ALG-3/4 pathway.

LITERATURE CITED

Afgan, E., D. Baker, M. van den Beek, D. Blankenberg, D. Bouvier *et al.*, 2016 The Galaxy platform for accessible, reproducible and collaborative biomedical analyses: 2016 update. Nucleic Acids Res. 44: W3–W10. https://doi.org/10.1093/nar/gkw343

Argon, Y., and S. Ward, 1980 Caenorhabditis elegans fertilization-defective mutants with abnormal sperm. Genetics 96: 413–433.

Arribere, J. A., R. T. Bell, B. X. H. Fu, K. L. Artiles, P. S. Hartman *et al.*, 2014 Efficient Marker-Free Recovery of Custom Genetic Modifications with CRISPR/Cas9 in Caenorhabditis elegans. Genetics 198: 837–846. https://doi.org/10.1534/genetics.114.169730

Baum, D. A., and B. Baum, 2014 An inside-out origin for the eukaryotic cell. BMC Biology 2014 12:1 12: 1. https://doi.org/10.1186/s12915-014-0076-2

Berndt, J. D., A. Aoyagi, P. Yang, J. N. Anastas, L. Tang *et al.*, 2011 Mindbomb 1, an E3 ubiquitin ligase, forms a complex with RYK to activate Wnt/β-catenin signaling. J. Cell Biol. 194: 737–750. https://doi.org/10.1083/jcb.201107021

Brenner, S., 1974 The genetics of Caenorhabditis elegans. Genetics. 77: 71–94.

Browning, H., and S. Strome, 1996 A sperm-supplied factor required for embryogenesis in C. elegans. Development 122: 391–404.

Conine, C. C., J. J. Moresco, W. Gu, M. Shirayama, D. Conte, Jr *et al.*, 2013 Argonautes Promote Male Fertility and Provide a Paternal Memory of Germline Gene Expression in C. elegans. Cell 155: 1532–1544. https://doi.org/10.1016/j.cell.2013.11.032

Dickinson, D. J., A. M. Pani, J. K. Heppert, C. D. Higgins, and B. Goldstein, 2015 Streamlined Genome Engineering with a Self-Excising Drug Selection Cassette. Genetics 200: 1035–1049. https://doi.org/10.1534/genetics.115.178335

Greenwald, I., 2005 LIN-12/Notch signaling in C. elegans, WormBook, ed. The C. elegans Research Community, WormBook, doi/10.1895/wormbook.1.10.1. http://www.wormbook.org.

Guo, B., B. J. McMillan, and S. C. Blacklow, 2016 Structure and function of the Mind bomb E3 ligase in the context of Notch signal transduction. Curr. Opin. Struct. Biol. 41: 38–45. https://doi.org/10.1016/j.sbi.2016.05.012

Hetzer, M. W., 2010 The Nuclear Envelope. Cold Spring Harb. Perspect. Biol. 2: a000539. https://doi.org/10.1101/cshperspect.a000539

Hirsh, D., D. Oppenheim, and M. Klass, 1976 Development of the reproductive system of Caenorhabditis elegans. Dev. Biol. 49: 200–219. https://doi.org/10.1016/0012-1606(76)90267-0

Hodgkin, J., 1993 Molecular cloning and duplication of the nematode sex-determining gene tra-1. Genetics 133: 543–560.

Itoh, M., C.-H. Kim, G. Palardy, T. Oda, Y.-J. Jiang *et al.*, 2003 Mind bomb is a ubiquitin ligase that is essential for efficient activation of Notch signaling by Delta. Dev. Cell 4: 67–82. https://doi.org/10.1016/S1534-5807(02)00409-4

Jaramillo-Lambert, A., M. Ellefson, A. M. Villeneuve, and J. Engebrecht, 2007 Differential timing of S phases, X chromosome replication, and meiotic prophase in the C. elegans germ line. Dev. Biol. 308: 206–221. https://doi.org/10.1016/j.ydbio.2007.05.019

Justine, J.-L., 2002 Male and Female Gametes and fertilisation, pp. 73–120 in *The Biology of Nematodes*, CRC Press, Boca Raton, FL.

Kang, K., D. Lee, S. Hong, S.-G. Park, and M.-R. Song, 2013 The E3 Ligase Mind Bomb-1 (Mib1) Modulates Delta-Notch Signaling to Control Neurogenesis and Gliogenesis in the Developing Spinal Cord. J. Biol. Chem. 288: 2580–2592. https://doi.org/10.1074/jbc.M112.398263

Koo, B.-K., K.-J. Yoon, K.-W. Yoo, H.-S. Lim, R. Song *et al.*, 2005 Mind Bomb-2 Is an E3 Ligase for Notch Ligand. J. Biol. Chem. 280: 22335–22342. https://doi.org/10.1074/jbc.M501631200

L'Hernault, S. W., D. C. Shakes, and S. Ward, 1988 Developmental genetics of chromosome I spermatogenesis-defective mutants in the nematode Caenorhabditis elegans. Genetics 120: 435–452.

Luxán, G., J. C. Casanova, B. Martínez-Poveda, B. Prados, G. D'Amato *et al.*, 2013 Mutations in the NOTCH pathway regulator MIB1 cause left ventricular noncompaction cardiomyopathy. Nat. Med. 19: 193–201. https://doi.org/10.1038/nm.3046

McNally, K. L. P., A. S. Fabritius, M. L. Ellefson, J. R. Flynn, J. A. Milan *et al.*, 2012 Kinesin-1 Prevents Capture of the Oocyte Meiotic Spindle by the Sperm Aster. Dev. Cell 22: 788–798. https://doi.org/10.1016/j.devcel.2012.01.010

Minevich, G., D. S. Park, D. Blankenberg, R. J. Poole, and O. Hobert, 2012 CloudMap: a cloud-based pipeline for analysis of mutant genome sequences. Genetics 192: 1249–1269. https://doi.org/10.1534/genetics.112.144204

Paix, A., A. Folkmann, D. Rasoloson, and G. Seydoux, 2015 High Efficiency, Homology-Directed Genome Editing in Caenorhabditis elegans Using CRISPR-Cas9 Ribonucleoprotein Complexes. Genetics 201: 47–54. https://doi.org/10.1534/genetics.115.179382

Paix, A., H. Schmidt, and G. Seydoux, 2016 Cas9-assisted recombineering in C. elegans: genome editing using in vivo assembly of linear DNAs. Nucleic Acids Res. 44: e128. https://doi.org/10.1093/nar/gkw502

Pavelec, D. M., J. Lachowiec, T. F. Duchaine, H. E. Smith, and S. Kennedy, 2009 Requirement for the ERI/DICER Complex in Endogenous RNA Interference and Sperm Development in Caenorhabditis elegans. Genetics 183: 1283–1295. https://doi.org/10.1534/genetics.109.108134

Ratliff, M., K. L. Hill-Harfe, E. J. Gleason, H. Ling, T. L. Kroft *et al.*, 2018 MIB-1 Is Required for Spermatogenesis and Facilitates LIN-12 and GLP-1 Activity in Caenorhabditis elegans. Genetics 209: 173–193. https://doi.org/10.1534/genetics.118.300807

Reinke, V., I. S. Gil, S. Ward, and K. Kazmer, 2004 Genome-wide germline-enriched and sex-biased expression profiles in Caenorhabditis elegans. Development 131: 311–323. https://doi.org/10.1242/dev.00914

Sadler, P. L., and D. C. Shakes, 2000 Anucleate Caenorhabditis elegans sperm can crawl, fertilize oocytes and direct anterior-posterior polarization of the 1-cell embryo. Development 127: 355–366.

Stiernagle, T., 2006 Maintenance of *C. elegans* (February 11, 2006), WormBook, ed. The *C. elegans* Research Community, WormBook, doi: 10.1895/wormbook.1.101.1. https://doi.org/10.1895/wormbook.1.101.1

Stoeckius, M., D. Grün, and N. Rajewsky, 2014 Paternal RNA contributions in the Caenorhabditis elegans zygote. EMBO J. 33: 1740–1750. https://doi.org/10.15252/embj.201488117

Ward, S., Y. Argon, and G. A. Nelson, 1981 Sperm morphogenesis in wild-type and fertilization-defective mutants of Caenorhabditis elegans. J. Cell Biol. 91: 26–44. https://doi.org/10.1083/jcb.91.1.26

Wolf, N., D. Hirsh, and J. R. McIntosh, 1978 Spermatogenesis in males of the free-living nematode, Caenorhabditis elegans. J. Ultrastruct. Res. 63: 155–169. https://doi.org/10.1016/S0022-5320(78)80071-9

Yushin, V. V., and V. V. Malakhov, 2014 The origin of nematode sperm: Progenesis at the cellular level. Russ. J. Mar. Biol. 40: 71–81. https://doi.org/10.1134/S1063074014020114

Communicating editor: D. Fay